ELSEVIER

Ceramics International 30 (2004) 239–249

CERAMICS INTERNATIONAL

www.elsevier.com/locate/ceramint

Reconstructive phase formation of ZrO_2 nanoparticles in a new orthorhombic crystal structure from an energized porous $ZrO(OH)_2{\cdot}xH_2O$ precursor

A. Mondal, S. Ram*

Materials Science Centre, Indian Institute of Technology, Kharagpur-721 302, India

Received 25 February 2003; received in revised form 12 April 2003; accepted 5 May 2003

Abstract

A high energy amorphous $ZrO(OH)_2{\cdot}xH_2O$ precursor (porous) is obtained by a controlled hydrolysis of dispersed Zr^{4+} cations in an aqueous solution in reaction with NH_4OH at 5 °C followed by aging and drying of the recovered gel at room temperature. At 20–40 °C in air, the excess H_2O evaporates leaving behind a porous $ZrO(OH)_2{\cdot}xH_2O$ powder with $\Phi \sim 37\%$ porosity. X-ray diffraction characterizes its amorphous structure with two halos at 20.8 and 36.7 nm^{-1} wavevectors. On heating, a reconstructive ZrO_2 phase transformation occurs from a refined amorphous state at 500 °C to form a new orthorhombic structure with $a = 0.3340$, $b = 0.5535$ and $c = 0.6364$ nm lattice parameters. Average crystallite size is $D \sim 15$ nm. This irreversibly transforms to m-ZrO_2 at $D \geqslant 23$ nm at 800 °C or above. A schematic energy level diagram for the precursor and the metastable ZrO_2 polymorphs is proposed with the observation of the phase transformations.

Keywords: A. Powder: chemical preparation; A. Grain growth; D. ZrO_2; Nanoceramics; Amorphous materials; Critical phenomena-phase tranformations

1. Introduction

Zirconia (ZrO_2) presents one of the most important and widely used high temperature structural and electronic ceramics [1–13]. The number of applications is growing with the fast advance of technology. The main drawback is, however, the thermal instability of its crystalline structures. At ambient pressure, it exists in a cubic (c) fluorite structure (O_h^5: Fm3m space group) at temperatures above 2370 °C, in O_{4h}^{15}: $P4_2/nmc$ tetragonal (t) structure at intermediate 1170–2370 °C temperatures, and in O_{2h}^5: $P2_1/c$ monoclinic (m) structure at temperatures below 950 °C [6–8]. The t- or c-phase derived from the m-phase can not be quenched to room temperature [8]. A doping with MgO, CaO, Y_2O_3, or similar other oxides stabilizes them at lower temperatures [8–13] in a high-energy microstructure at manifested total surface (Ω) and/or Gibbs free (G) energies in small crystallites over the equilibrium bulk m-phase.

Under pressure, ZrO_2 transforms to a series of orthorhombic (o) phases [14,15]. The first one (Pbca space group) starts at an applied pressure of ~3 GPa depending upon the grain size and is observed to exist up to ~22 GPa when another o-phase (Pnam cotunnite structure) sets in. A third $Pbc2_1$ o-phase has been observed in some cases of partially stabilized ZrO_2. The o-ZrO_2 crystal structures are very similar to the tetragonal one but in a higher symmetry [14,15].

Moreover, it is observed that during milling m-ZrO_2 transforms to a metastable t-ZrO_2 phase [16] or a new o-ZrO_2 phase [17]. Addition of an excess energy or volume, at early milling stages in refining the structure with high energy grain boundaries and defects, destabilizes the m-ZrO_2 structure at a critical grain size $D = D_c$, i.e. found to be 12.3 nm [17]. The latter precipitates o-ZrO_2 in small particles (in energy very close to that in a destabilized amorphous structure) by optimizing the total energy to an equilibrium value. Molodetsky et al. [18] recrystallized t-ZrO_2 from an amorphous $ZrO(OH)_2{\cdot}xH_2O$ precursor, obtained by hydrolysis of Zr^{4+} with NH_4OH in water, by heating it at 350 °C for 2 h. Xie [19] has been successful in synthesizing a transparent $ZrO(OH)_2{\cdot}xH_2O$ gel by Zr^{4+} hydrolysis with

* Corresponding author. Tel.: +091-3222-283980/283981; fax: +091-3222-255303/282700.
E-mail address: sram@matsc.iitkgp.ernet.in (S. Ram).

0272-8842/03/$30.00
doi:10.1016/S0272-8842(03)00095-6

ethylene oxide C_2H_4O in water. An ultrafine ZrO_2 powder, $D \sim 12$ nm, results after the gel is dried and calcined at 600 °C. This is the minimum temperature necessary to decompose the gel and to remove the byproducts. It appears in the m-phase only.

In exploring such metastable phases, this work studies an energized porous $ZrO(OH)_2{\cdot}xH_2O$ precursor, obtained by a controlled hydrolysis of dispersed Zr^{4+} cations with NH_4OH in water followed by drying and pulverizing the recovered gel at room temperature. It results in a monolithic o-ZrO_2, $D \sim 15$ nm, at 500 °C. The results are analyzed and discussed with X-ray diffraction, microstructure, thermogravimetric analysis, and IR spectrum.

2. Experimental details

2.1. Synthesis of the $ZrO(OH)_2{\cdot}xH_2O$ precursor

A monolithic $ZrO(OH)_2{\cdot}xH_2O$ precursor was synthesized by the hydrolysis of dispersed Zr^{4+} cations with NH_4OH in an aqueous solution. A stock solution of zirconyl oxychloride, $ZrOCl_2{\cdot}8H_2O$, in distilled water in 0.5 M concentration was used. NH_4OH, dissolved in water (28%), was added dropwise while stirring the mixture with a magnetic stirrer at 5 °C (controlled by a low temperature liquid bath of Julabo model HD-4). Average pH was maintained at ~10. A glassy gel $ZrO(OH)_2{\cdot}xH_2O$ appears of hydrolyzed Zr^{4+} after 10–20 min of the reaction. It was filtered and dispersed in distilled water to remove byproduct impurities. The absence of NH_4^+ in the recovered sample was confirmed by Nessler's test as was that of Cl^- by using $AgNO_3$.

The recovered sample was dried in two batches in air at (i) room temperature and (ii) 80–150 °C over a sand bath. To facilitate the evaporation, the sample (i) was dispersed over a porous porcelain disk with 1–2 mm pore diameter. A dried and pulverized powder of porous $ZrO(OH)_2{\cdot}xH_2O$ results on evaporation of the excess H_2O in air over a period of a month or so at room temperature (Table 1). Hydrated zirconia, $ZrO_2{\cdot}xH_2O$, is the dried precursor in experiment (ii). Both the $ZrO(OH)_2{\cdot}xH_2O$ and the $ZrO_2{\cdot}xH_2O$ are amorphous in structure.

A refined ZrO_2 nanopowder occurs on dehydrating and decomposing $ZrO(OH)_2{\cdot}xH_2O$ precursor at temperature as low as 200 °C in air. Its structure, especially if processed at low temperature, depends on the initial precursor structure. A porous precursor, with a significantly excess volume, involves an altogether different structure in a high-energy metastable state G_p^p above the equilibrium value. As a result, it passes through a modified sequence of reconstructive phase transformations as per its excess energy and thermodynamics. The whole process is shown schematically in Fig. 1.

2.2. Characteristic measurements

The porous structure of the precursor powder has been confirmed by the N_2 gas sorption and by difference in its measured (by displacement method in toluene) and theoretical values of density ρ. Amorphous or crystalline structure of the initial precursor or its derivative of ZrO_2 after a reconstructive phase transformation from it is analyzed by X-ray diffraction. The diffractogram has been recorded on PHILIPS P.W. 1710 diffractometer using filtered CoK_α radiation of wavelength $\lambda = 0.17905$ nm. $ZrO(OH)_2{\cdot}xH_2O \rightarrow (1+x)H_2O + ZrO_2$ molecular decomposition and formation of ZrO_2 from the precursor were studied with TG-DTA thermogravimetric and differential thermal analysis using a Perkin-Elmer thermal analyzer (Model DT- 40, Shimadzu Co. Kyoto, Japan). The data were collected by heating the sample in an argon atmosphere at a heating rate of 20 °C/min.

The size and morphology of ZrO_2 particles/crystallites in the powder were studied with a scanning electron microscope (SEM) of JEOL model-840 and a transmission electron microscope (TEM) of Philips CM-12 at 180 kV. For TEM observations, the sample powder was dispersed in acetone in an ultrasonic bath for 15 min. Then a small droplet from the suspension of the sample in the acetone was put over a carbon coated

Table 1
Structure, density ρ and porosity Φ in ZrO_2 powders derived from a porous $ZrO(OH)_2xH_2O$ precursor

	Sample	Structure	ρ (g/cm^3)	Φ (%)
(1)	Porous $ZrO(OH)_2{\cdot}xH_2O$	Amorphous	1.95	37
(2)	Nonporous wet $ZrO(OH)_2{\cdot}xH_2O$	Amorphous	3.10	
(3)	a-ZrO_2 after (1) at 300 °C, 2 h	Amorphous	3.25 (5.86)	45
(4)	ZrO_2 after (1) at 500 °C, 2 h	Orthorhombic	4.27 (6.96)	39
(5)	ZrO_2 after (1) at 800 °C, 2 h	Monoclinic	4.17 (5.86)	29
(6)	ZrO_2 after (2) at 200 °C, 5 h	Cubic	2.85 (6.15)	54
(7)	ZrO_2 after (2) at 500 °C, 2 h	Cubic	3.85 (6.18)	38
(9)	ZrO_2 after (2) at 800°, 2 h	Monoclinic	4.19 (5.82)	28

The theoretical ρ values are given in the parentheses. The Φ in sample (1) is obtained by difference of ρ (experimental) from the value in the parent sample (2). In lack of the actual theoretical ρ value, the same value as in m-ZrO_2 is taken for the a-ZrO_2.

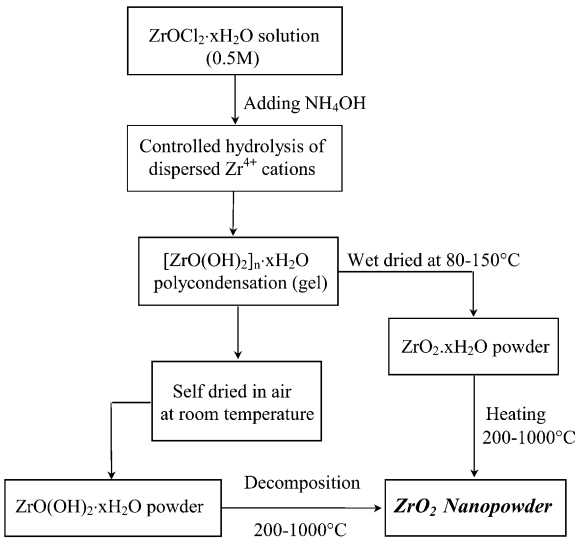

Fig. 1. A schematic diagram in hydrolysis and polycondensation of dispersed Zr^{4+} to an amorphous gel and reconstructive phase transformation to a ZrO_2 nanopowder.

copper grid specially made for the TEM analysis. An average D value is calculated from widths $\Delta 2\theta_{1/2}$ in the characteristic X-ray diffraction peaks with the Debye Scherrer relation [20]. IR spectrum (200–4000 cm^{-1}) has been studied of the powder in a KBr pellet with Shimadzu IR 470 spectrophotometer. The reported frequencies are accurate to ± 2 cm^{-1} in the case of sharp bands and ± 5 cm^{-1} or even larger in the case of broad bands.

3. Results and discussion

3.1. Hydrolysis reaction process

The addition of NH_4OH, under the controlled conditions at 5 °C, promotes spontaneous hydrolysis of Zr^{4+} cations in the $ZrOCl_2$ solution to form $ZrO(OH)_2{\cdot}xH_2O$. Dispersed molecules of $ZrOCl_2$, which are ionic in nature, react with H_2O as per the reaction,

$$ZrOCl_2 + 2H_2O \rightarrow ZrO(OH)_2 + 2HCl, \quad (1)$$

which proceeds if the HCl reacts. This is satisfied with NH_4OH as it reacts instantaneously with HCl and forms NH_4Cl. As a result, the ionic strength of the solution does not increase during the reaction. In controlled reaction conditions, as soon as the nascent $ZrO(OH)_2$ molecules appear recombine one another with H_2O molecules in a specific fashion by so called "polymerization or polycondensation". This appears in a transparent amorphous gel,

$$nZrO(OH)_2 \xrightarrow{xH_2O} \left[ZrO(OH)_2\right]_n{\cdot}xH_2O. \quad (2)$$

In comparison to obtain a similar hydrolyzed gel by the conventional sol-gel process with zirconium alkoxide, this is a very simple and easily controlled process. It represents a new sol-gel process for preparing a polymeric $[ZrO(OH)_2]_n{\cdot}xH_2O$ gel with dispersed Zr^{4+} cations in water. In the virgin sol-gel method, the starting material for conducting the hydrolysis process is usually zirconium isopropoxide $Zr(i\text{-}OC_3H_7)_4$, zirconium propoxide $Zr(n\text{-}OC_2H_7)_4$, or zirconium butoxide $Zr(n\text{-}OC_4H_9)_4$ [19,21]. Obviously, this process is complicated and difficult to control. Zirconium alkoxides are generally derived from $ZrCl_4$ and kept away from water [21].

A different reaction process occurs in a complex manner if adding NH_4OH to $ZrOCl_2$ solution a rather fast at room temperature without extensive stirring. A stable precipitate forms of $Zr(OH)_4{\cdot}xH_2O$ in a different whitish characteristic colour. The reaction mixture suffers from a manifested local ionic strength in inhomogeneous distribution of excess H^+ and OH^-. This disrupts $ZrO(OH)_2$ polycondensation in reactions (1) and (2). As an alternative to attain the equilibrium, a local $ZrO(OH)_2 + H^+ + OH^- \rightarrow Zr(OH)_4$ reaction occurs. This is the reason that several authors reported $Zr(OH)_4$ as the end product in such reactions [18,22,23]. It is not so stable and transforms to hydrated zirconia, $Zr(OH)_4 \rightarrow ZrO_2{\cdot}2H_2O$, even at room temperature.

Zr^{4+} has a high covalency and seven coordination-bonding characteristics, which are rare in other transition metal cations [24]. It thus forms all three types of covalent, ionic, and interstitial bonds. Cotton and Wilkinson [25] studied the Zr^{4+} bonding behavior in aqueous solution with the conclusion that $Zr(OH)_4$ is non-existent and rather converts to $ZrO_2{\cdot}\alpha H_2O$. It does not form cationic complexes of any kind. It is doubtful if any simple aquo-Zr^{4+} cation exists even in a strong acid solution. The simple Zr^{4+} salts thus could be regarded either as covalent molecules, such as $ZrCl_4$ and $Zr(CH_3COO)_4$, or as complex anions, such as $[Zr(SO_4)_3]^{2-}$, $[ZrF_6]^{2-}$ and $[ZrF_7]^{3-}$. Our results confirms it that in solution Zr^{4+} forms primarily complexes, polynuclear compounds and polymers in which the Zr^{4+} mainly covalently bonds.

On drying in air at room temperature, the $[ZrO(OH)_2]_n{\cdot}xH_2O$ gel desorbs the excess water molecules leaving behind a refined porous powder. The obtained $[ZrO(OH_2)]_n{\cdot}xH_2O$ sample has reduced dimension at a micrometer scale ($n \sim 10^5$), with $x \leqslant 3$ (5–8 otherwise) as determined by the TG analysis. On the other hand, $Zr(OH)_4{\cdot}xH_2O$ does not form a stable $[Zr(OH)_4]_n{\cdot}xH_2O$ structure. It involves a weak Zr–Zr (Zr–O–Zr otherwise) bonding between the monomers and thus rather easily decomposes to $ZrO_2{\cdot}xH_2O$.

3.2. Reaction in refined metastable ZrO_2 structures

A metastable ZrO_2 structure appears by a controlled reconstructive thermal decomposition from a high energy $ZrO(OH)_2{\cdot}xH_2O$ precursor. It is the size and

internal structure of precursor that govern not only its decomposition process but also the reconstruction from reaction of its decomposed species. As per the experimental conditions of the reaction species and other parameters, the reaction passes through a series of high-energy metastable ZrO_2 structures, approaching the equilibrium G_e^m value. Thermodynamics and decomposition process of precursor determine the energy and local structure in the reaction species.

A primary method of deriving a specific phase out of the equilibrium is to decompose the processor at an elevated temperature and allow the latter to have a controlled reconstructive reaction. The temperature should be sufficient enough to complete the decomposition and to remove the byproducts (here water molecules only). Unfortunately, this often leads to a fast grain growth of product. To plan a sintering strategy to encourage decomposition without simultaneously stimulating grain growth is not so easy. This is what needed here in a metastable structure of ZrO_2 in a strictly controlled size in a few nanometers.

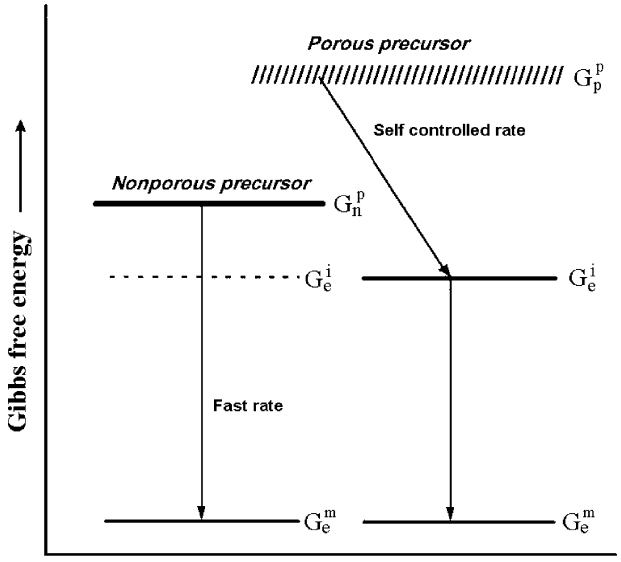

Fig. 2. A schematic diagram in a self-controlled reconstructive phase formation in a metastable ZrO_2 phase G_e^i through a high-energy porous precursor G_p^p. A fast transformation in a nonporous precursor G_n^p leads to the equilibrium phase G_e^m in a single step.

One well-known strategy is simply to add a solute or second phase particles to a monolithic ZrO_2 phase to reduce grain boundary mobilities or to pin grain boundaries [26]. Nanopores in a porous precursor serve a similar purpose. An advantage with it is that it causes no change in the basic chemical composition of the sample. Excess volume in pore raises average volume V, and in turn the G value, of the specimen above the equilibrium G_e^m value in a metastable state G_p^p. On heating, the excess volume $\Delta V_i = V_p^p - V_e^i$ relative to a metastable state G_e^i releases at temperature T_i, and the system appears in this state. This occurs in a thermodynamically self-controlled manner through pores. As shown in Fig. 2, a reasonably fast ΔV_i release, as in a nonporous precursor, drives an effectively fast $G_n^p \rightarrow G_e^m$ phase transformation to the bulk state in a single step.

3.3. Thermogravimetric and IR spectral analyses

TG-DTA curves (Fig. 3) in porous $ZrO(OH)_2 \cdot xH_2O$ has an endothermic peak at 85 °C and an exothermic peak at 451 °C, at a heating rate of $\beta = 20$ °C/min, with a total of 35.8% mass loss as per $x = 2.81$. Most of the mass loss of 32% occurs as early as to 240 °C in desorption of the internal water and $ZrO(OH)_2$ molecular decomposition to ZrO_2 in the endothermic signal. The residual 3.8% value imparts by desorption of re-adsorbed water in porous ZrO_2 over higher temperatures. Part of the water,

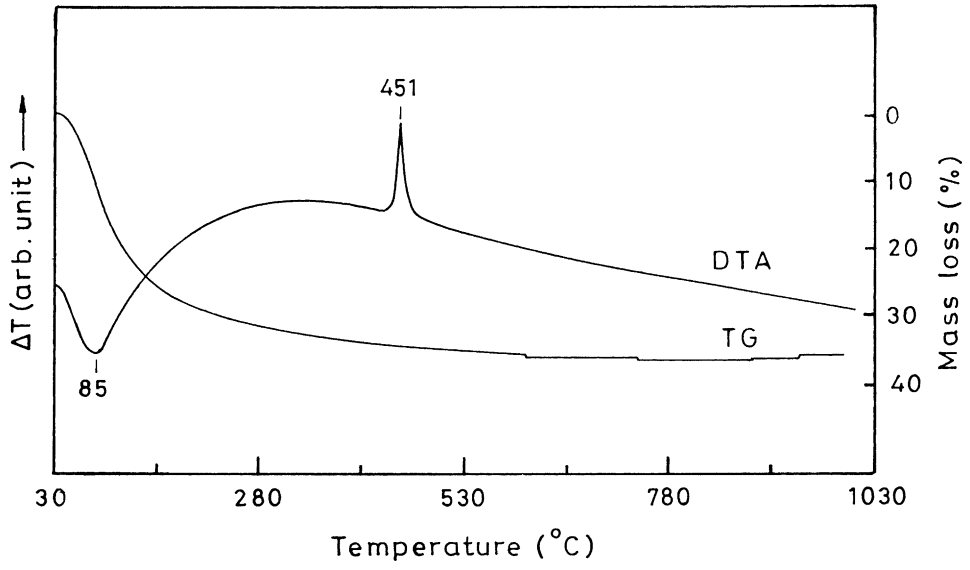

Fig. 3. TG-DTA thermograms for porous $ZrO(OH)_2 \cdot xH_2O$ precursor at a heating rate of 20 °C/min (in an argon atmosphere).

which comes out on decomposing $ZrO(OH)_2$, gets adsorbed in the resulting refined ZrO_2 and that relieves at these temperatures. As will be discussed later, it favors an activated reconstructive ZrO_2 nucleation and growth.

Osendi et al. [2] reported a modified endothermic peak in TG-DTA (at $\beta = 10$ °C/min) at 150 °C in precipitated $ZrO(OH)_2{\cdot}xH_2O$ by reaction of $ZrOCl_2$ with NH_4OH in water at room temperature. The exothermic peak (refers to recrystallization of the amorphous a-ZrO_2 powder) lies at a bit smaller 412 °C value, with a limited 20% mass loss as per a value of $x = 0.71$. In our porous $ZrO(OH)_2{\cdot}xH_2O$ sample, a plenty of chemisorbed H_2O molecules in pores and high energy molecular surfaces distributed through pores support molecular decomposition of it at moderate 85 °C temperature. The pores control the reaction in refined species after the decomposition so that it occurs at extended 451 °C temperature.

A chemidesorption of adsorbed species or a chemical decomposition is an endothermic process. It occurs by absorbing heat to raising the enthalpy of the system to a critical limit of its thermodynamic stability before it dissociates. This is very much reflected in by the desorption of structural or chemisorbed H_2O molecules and the $ZrO(OH)_2$ molecular decomposition. The two processes are interrelated through H-bonding. A nucleation and growth in ZrO_2 by a reaction of decomposed precursor species is an altogether exothermic in nature. It thus occurs with a well-defined exothermic peak at 451 °C.

IR spectrum (Fig. 4a) of two O–H stretching bands at 3445 and 2933 cm^{-1} and three O–H bending bands at 1723,1636 and 1545 cm^{-1} characterizes the $[ZrO(OH)_2]_n{\cdot}xH_2O$ polymer structure. Weak bands at 1070 and 1021 cm^{-1} describe the Zr=O group stretching vibrations. One Zr=O group may result in two stretching vibrations in two $ZrO(OH)_2$ conformers. In

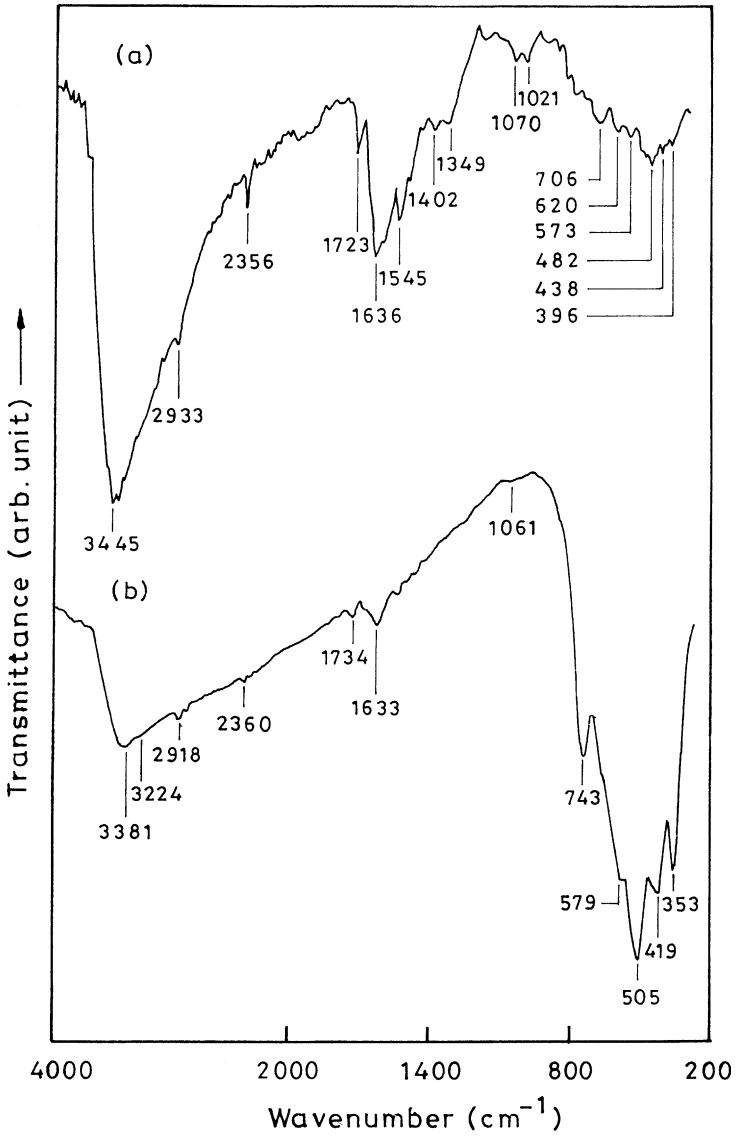

Fig. 4. IR spectra for porous (a) $ZrO(OH)_2{\cdot}xH_2O$ and (b) o-ZrO_2 after (a) at 500 °C for 2 h.

$[ZrO(OH)_2]_n \cdot xH_2O$ polymer, most of the Zr=O bonds have converted to Zr–O bonds as inferred by weak intensities in the two bands. Other bands in the 300–1000 cm^{-1} and 1300–2500 cm^{-1} regions refer to O–H deformation vibrations, H_2O lattice vibrations, and the combination bands. New bands occur at 743, 579, 505, 419 and 353 cm^{-1} (Fig. 4b) after decomposition of precursor to o-ZrO_2 at 500 °C in 2 h. They are characteristic of Zr–O stretching and bending vibrations of ZrO_2 in ZrO_δ, usually $\delta = 4$ and 6, polyhedron [1,3].

Significantly different bands at 730, 588, 520, 445, 420 and 350 cm^{-1} have been reported in m-ZrO_2 [3]. A broad characteristic band at 550–650 cm^{-1} appears in t-ZrO_2 while at 628 cm^{-1} in c-ZrO_2 [1,3]. In general, all the four ZrO_2 polymorphs have very similar vibrational structures. A minor variation in their frequencies or relative intensities occurs in different Zr^{4+} distribution in the interstitial sites. They are sensitive to the oxygen vacancies and other defects.

3.4. X-ray diffraction

X-ray diffraction (Fig. 5a) in porous $ZrO(OH)_2 \cdot xH_2O$ has two broad halos at wavevectors $q_1 = 20.8$ and $q_2 = 36.7$ nm^{-1} with $\Delta 2\theta_{1/2} = 12.1$ and 22.4°, respectively, in amorphous structure with two prominent pair distribution functions of atoms [27,28]. Halo q_2 has an improved intensity (integrated) I_t by ~5% relative to halo q_1, which is the most prominent with $I_t \sim 70\%$ value in two halos, on heating the sample at 300 °C for 2 h (Fig. 5b). The two halos lie at $q_1 = 21.0$ ($\Delta 2\theta_{1/2} = 13.6°$) and $q_2 = 37.1$ ($\Delta 2\theta_{1/2} = 22.5°$) nm^{-1} in a wet precursor, with I_t ~15% in halo q_1 (as compared in the inset to Fig. 5). The minor variation in position or I_t in q_i demonstrates a minor variation in the pair distribution functions in the samples.

A recrystallization from a-ZrO_2 results in well defined X-ray diffraction peaks on heating from the porous $ZrO(OH)_2 \cdot xH_2O$ at 500 °C for 2 h. It is a new diffractogram (Fig. 6) in comparison to those of well known in the c-, t- or m-ZrO_2 [29]. Most of these peaks differ in positions and/or relative intensities I_p from those in these polymorphs. The most intense peak lies at 0.2955 nm ($I_p = 100$ units) with the second and third most intense ones at 0.3165 ($I_p = 63$ units) and 0.1812 nm ($I_p = 62$ units), respectively. The 0.3165 nm peak by chance compares in position the most intense ($11\bar{1}$) peak in m-ZrO_2 at 0.3160 nm [29], but this is not from m-ZrO_2 as its second most intense (111) peak is absent at 0.2830 nm. Moreover, (111), (220) and (311) three characteristic peaks of c-ZrO_2 at 0.2930, 0.1801 and 0.1534 nm are in poor comparison with the peaks at 0.2955, 0.1812 and 0.1547 nm. This has a much simple diffractogram of a total of only ten peaks in this range, with the most intense peak of 0.2930 nm (111), which is absent here. None of the observed peaks is matching with t-ZrO_2 peaks. The most intense peak of it lies in (101) reflection at an altogether different 0.2995 nm value [29].

All of the observed peaks in diffractogram in Fig. 6 are indexed (Table 2) assuming o-ZrO_2 polymorph with

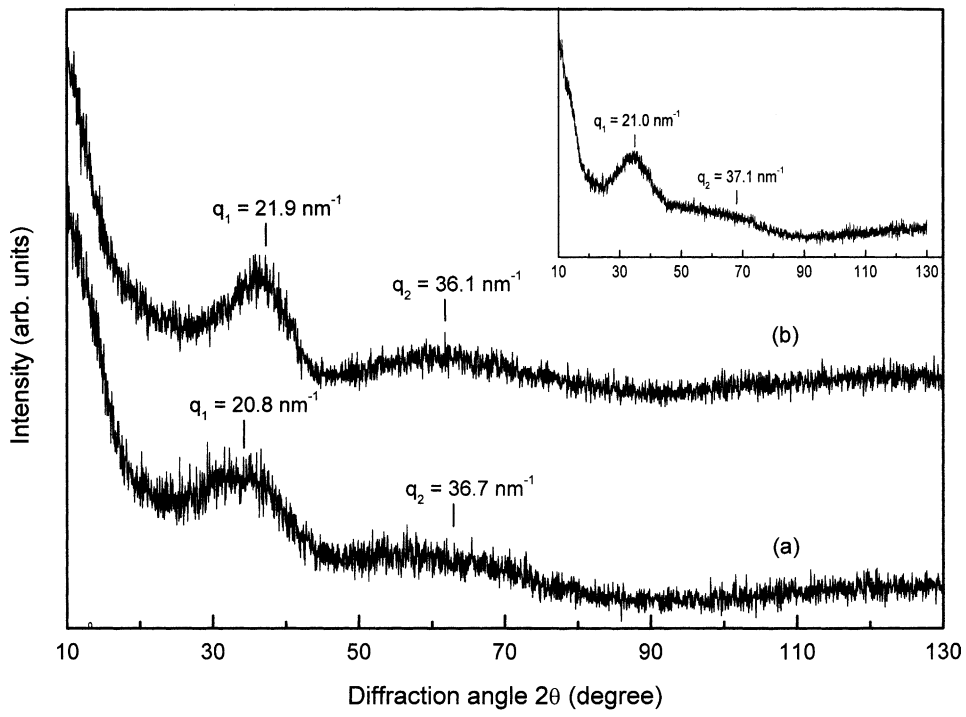

Fig. 5. X-ray diffractograms in porous (a) $ZrO(OH)_2 \cdot xH_2O$ and (b) a-ZrO_2 after (a) at 300 °C for 2 h. Diffractogram from a wet $ZrO(OH)_2 \cdot xH_2O$ precursor powder is compared in the inset.

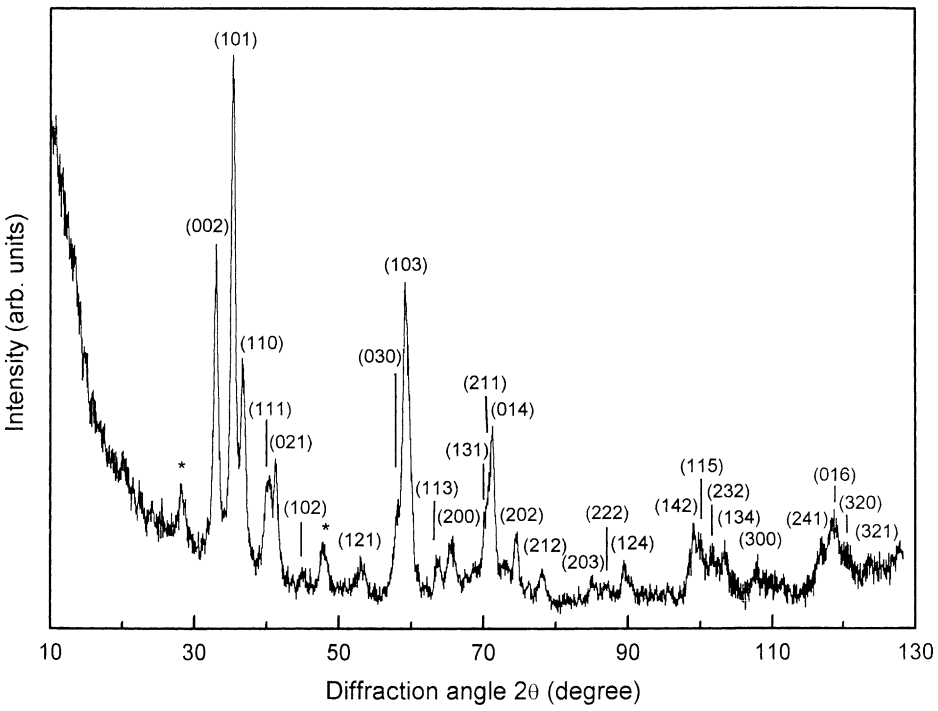

Fig. 6. X-ray diffractogram in o-ZrO_2 nanopowder from porous $ZrO(OH)_2{\cdot}xH_2O$ at 500 °C for 2 h. *Unidentified peaks.

lattice parameters $a=0.3340$, $b=0.5535$ and $c=0.6364$ nm. The d_{hkl} (interplanar spacing) values are reproduced within a standard deviation of ± 0.0010 nm, i.e. the error of the measurement, as per the relation [30],

$$\frac{1}{d_{hkl}^2}=\frac{h^2}{a^2}+\frac{k^2}{b^2}+\frac{1^2}{c^2} \quad (3)$$

The most intense 0.2955 nm peak of the diffractogram is fairy matching with the calculated value of 0.2957 nm in (101) reflection. As an exception, the (103) and (002) peaks at 0.1812 and 0.3165 nm have a rather large deviation of 0.0021 and 0.0017 nm from the calculated ones, possibly in the lattice distortion. The unit cell volume $V_0=0.1177$ nm^3 gives $\rho=6.96$ g/cm^3 density with $Z=4$ ZrO_2 molecules per unit cell. The value of $\rho=6.15$ g/cm^3 at $Z=4$ in the cubic lattice or $\rho=5.86$ g/cm^3 at $Z=4$ in the monoclinic lattice (Table 3).

As can be seen from the X-ray diffraction in Fig. 7 the metastable phase of o-ZrO_2 converts to m-ZrO_2 by an increase in D from 15 to 23 nm (analyzed from the $\Delta 2\theta_{1/2}$ values) on heating at 800 °C for 2 h. The lattice parameters are $a=0.5143$ nm, $b=0.5194$ nm, $c=0.5298$ nm, and $\beta=99°23'$ against the $a=0.5148$ nm, $b=0.5203$ nm, $c=0.5316$ nm and $\beta=99°23'$ bulk values [29]. A similar result appears if heating the precursor directly to 800 °C for 2 h and then cooling to room temperature. Even in so small D it is stable and does not revert back to o-ZrO_2 or other metastable polymorphs during the cooling at lower temperatures.

A modified c-ZrO_2 phase formation occurs by a wet $ZrO(OH)_2{\cdot}xH_2O$ at moderate 200 °C temperature. It seems that the H_2O molecules, which become mobile during heating at early temperatures, energize the Zr^{4+} and O^{2-} reaction species so that they have an activated reaction in c-ZrO_2 at these temperatures. Fig. 8 shows X-ray diffractogram in a pure c-ZrO_2 obtained in 5 h of heating at 200 °C by this precursor. It has a self-controlled $D=8$ nm in a bit enhanced lattice parameter $a=0.5105$ nm relative to the 0.5090 nm bulk value [29]. The enhanced a demonstrates the fact of a significantly enhanced d_{hkl} in small crystallites [31]. A lower $D=22$ nm value, in comparison to the 23 nm obtained by a porous precursor, occurs in m-ZrO_2 phase on raising the temperature at 800 °C (see the X-ray diffractogram in the inset in Fig. 8). The difference in D in the two samples is well demonstrated by a close-up of $(11\bar{1})$ peak in Fig. 7.

Murase and Kato [22] studied m- and t-ZrO_2 growth by heating ultrafine powders up to 1000 °C in a dry air and a wet atmosphere with water vapour. It has been found that the water vapour accelerates their growth. It facilitates t → m phase transformation at critical size D_c ~22 nm (~28 nm in dry air). At 1000 °C, $D=5$ nm m-ZrO_2 grows as big as 60 nm in the water vapour against 42 nm in the dry air. Possibly, the water vapour increases surface diffusion and thus enhances the grain growth. The t → m phase transformation is accelerated by (i) the acceleration of the grain growth by the manifested sur-

Table 2
Interplanar d_{hkl} spacings and relative intensities (I) in the peaks in X-ray powder diffraction for o-ZrO_2 nanopowder

d_{hkl} (nm)					
Observed	Calculated	I	h	k	l
0.3695		13			
0.3165	0.3182	63	0	0	2
0.2955	0.2957	100	1	0	1
0.2853	0.2860	42	1	1	0
0.2595	0.2608	21	1	1	1
0.2544	0.2538	24	0	2	1
0.2317	0.2304	2	1	0	2
0.2209		10			
0.2011	0.2021	6	1	2	1
0.1845	0.1845	17	0	3	0
0.1812	0.1791	62	1	0	3
0.1703	0.1704	6	1	1	3
0.1657	0.1670	11	2	0	0
0.1559	0.1565	15	1	3	1
0.1547	0.1551	20	2	1	1
0.1535	0.1529	34	0	1	4
0.1476	0.1479	12	2	0	2
0.1422	0.1429	5	2	1	2
0.1322	0.1312	2	2	0	3
0.1297	0.1304	4	2	2	2
0.1273	0.1275	7	1	2	4
0.1178	0.1186	12	1	4	2
0.1168	0.1163	10	1	1	5
0.1155	0.1154	9	2	3	2
0.1140	0.1133	9	1	3	4
0.1107	0.1113	3	3	0	0
0.1050	0.1051	9	2	4	1
0.1040	0.1042	12	0	1	6
0.1029	0.1033	8	3	2	0
0.1015	0.1019	2	3	2	1

The sample has been derived from the porous $ZrO(OH)_2{\cdot}xH_2O$ after heating at 500 °C for 2 h. The d_{hkl} values are calculated from the average lattice parameters $a=0.3340$ nm, $b=0.5535$ nm and $c=0.6364$ nm in an orthorhombic crystal structure.

face diffusion and (ii) the reduction in D_c by diminution in difference in the surface energies in the two phases.

3.5. Microstructure

SEM in (a) $ZrO(OH)_2{\cdot}xH_2O$ precursor (porous) and ZrO_2 powders after heating from it at (b) 300 °C, (c) 500 °C and (d) 800 °C for 2 h are compared in Fig. 9. Amorphous powders in (a) precursor and (b) the derived ZrO_2 at low temperature consist of thin platelet structures of 1 to 15 μm. The ZrO_2 platelets, which, of course, are clusters of finer particles, have reorganized in a refined structure of precursor. Near spherical shape of clusters, 200–500 nm diameter, are recrystallized in (c) and (d). As per the $\Delta 2\theta_{1/2}$ values, they consist of (c) 15 nm and (d) 23 nm crystallites. A spherical o-ZrO_2 crystallite involves a specific surface area $\Omega = 4\pi r^2 \div \frac{4}{3}\pi r^3\rho \equiv 3/r\rho$, i.e., ~ 58 m^2/g at $r = D/2 \equiv 7.5$ nm and $\rho = 6.96$ g/cm^3. It is as small as 20 times that in a 300 nm cluster in Fig. 9(c). Such a big cluster, in a close packing of crystallites by neglecting the interspacing, has as many crystallites as 8×10^3. At so low a temperature, insufficient to drive a fast grain growth, the high energy, $\Omega \sim 58$ m^2/g, crystallites with nascent surfaces, especially in presence of the adsorbed H_2O, rearrange in clusters by minimizing the average Ω value. A spherical shape of cluster is a direct consequence of it.

Table 3
Crystal structure, lattice number Z, lattice parameters, lattice volume V_0, and specific density ρ in the various ZrO_2 polymorphs

Polymorphs	Z	Lattice parameter (nm)		V_0 (nm^3)	ρ (g/cm^3)	Ref.
Ambient pressure						
c-ZrO_2	4	*a*	0.5105	0.1331 (0.1319)	6.15 (6.20)	This work
o-ZrO_2	4	*a*	0.3340	0.1177	6.96	This work
		b	0.5535			
		c	0.6364			
t-ZrO_2	2	*a*	0.3640	0.0698	5.86	[29b]
		c	0.5270			
m-ZrO_2	4	*a*	0.5143	0.1396 (0.1405)	5.86 (5.82)	This work
		b	0.5194			
		c	0.5298			
High pressure						
Orth-I Pbca	8	*a*	0.5067	0.2590	6.32	[10]
		b	0.5156			
		c	0.9915			
Orth-II Pnam	4	*a*	0.5587	0.1207	6.78	[10]
		b	0.6487			
		c	0.3330			

The standard V_0 and ρ values given in the parentheses are reported from Ref. [29].

Size and morphology of the ZrO_2 crystallites, which lie at a smaller scale, are studied with TEM (Fig. 10). Small o-ZrO_2 particles in TEM (a) are in platelet shapes, $D = 12$–18 nm, consistent with the 15 nm value determined from the $\Delta 2\theta_{1/2}$ values. They are assembled in clusters. $D = 20$–25 nm m-ZrO_2 crystallites are present in TEM (b) in agreement with the 23 nm value from the $\Delta 2\theta_{1/2}$ values. In fact, all the three ZrO_2 samples have mostly clusters of crystallites as observed in the SEM micrographs (Fig. 9). As usual, some of the independent crystallites still retain and those appeared in these TEM micrographs. The electron diffraction (c) corresponding to TEM (a) has five rings at 0.2954, 0.2601, 0.1806, 0.1530 and 0.1180 nm d_{hkl} values in (101), (111), (103), (014) and (142) reflections. They compare the 0.2955, 0.2595, 0.1812, 0.1535 and 0.1178 nm values in the X-ray diffractogram (Fig. 6). The electron diffraction (d) corresponding to TEM (b) has three rings at 0.3150, 0.2215 and 0.1801 nm d_{hkl} values, in agreement with the 0.3152, 0.2212 and 0.1801 nm values in the X-ray diffraction (Fig. 7), in $(11\bar{1})$, $(21\bar{1})$ and $(12\bar{2})$ reflections.

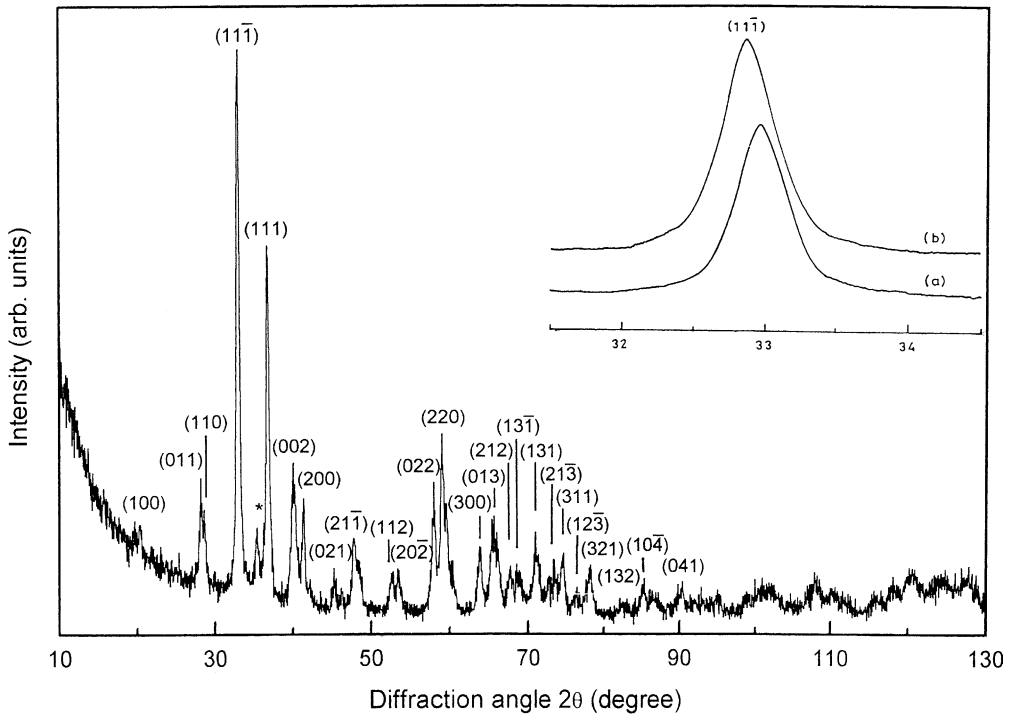

Fig. 7. X-ray diffractogram in m-ZrO_2 nanopowder from porous $ZrO(OH)_2{\cdot}xH_2O$ at 800 °C for 2 h. *(101) peak at 0.2944 nm in trace of t-ZrO_2. A close-up of (11$\bar{1}$) peak in the inset compares 2θ and $\Delta 2\theta_{1/2}$ values in the samples processed from (a) porous and (b) nonporous precursors.

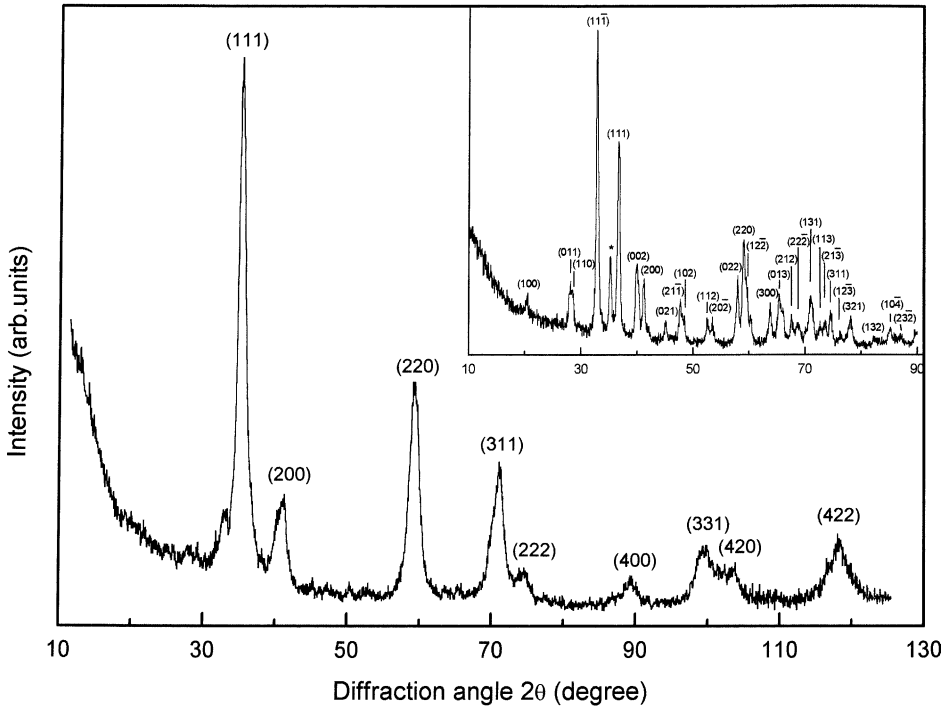

Fig. 8. X-ray diffractogram in c-ZrO_2 nanopowder from a wet $ZrO(OH)_2{\cdot}xH_2O$ precursor after heating at 200 °C for 5 h. Raising the temperature at 800 °C results in an m-ZrO_2 nanopowder in 2 h of diffractogram compared in the inset. *(101) peak at 0.2956 nm in trace t-ZrO_2.

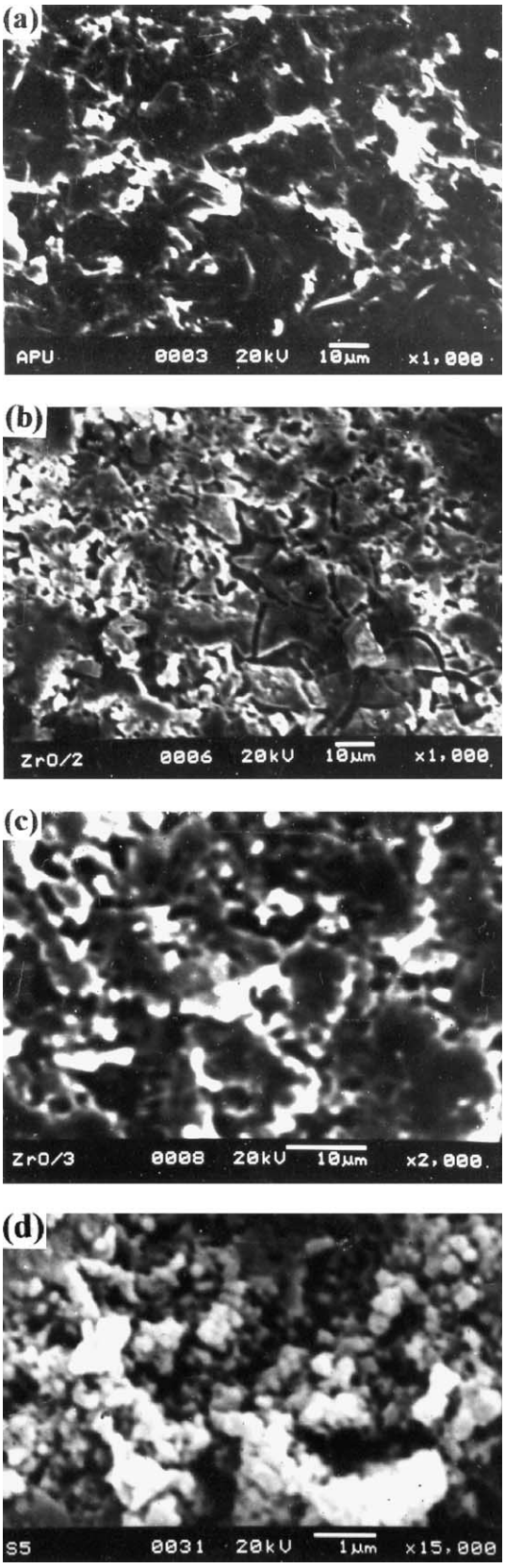

Fig. 9. SEM for (a) porous $ZrO(OH)_2 \cdot xH_2O$ and (b) a-ZrO_2, (c) o-ZrO_2, and (d) m-ZrO_2 nanopowders from (a) after heating at 300, 500, and 800 °C, respectively, for 2 h.

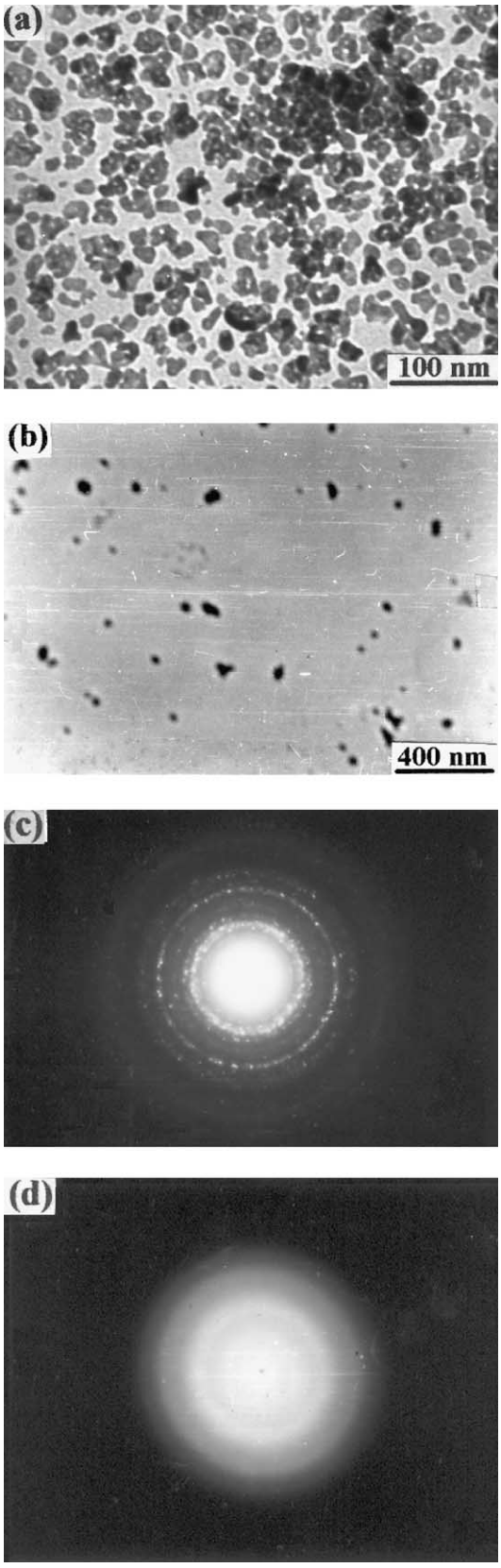

Fig. 10. TEM for (a) o-ZrO_2 and (b) m-ZrO_2 nanopowders in Fig. 9. (c) and (d) the electron diffraction corresponding to TEM (a) and (b) respectively.

4. Conclusions

A porous $ZrO(OH)_2{\cdot}xH_2O$ precursor (amorphous) is developed by a controlled hydrolysis and polycondensation of dispersed Zr^{4+} in water at 5 °C followed by drying the recovered gel in air at room temperature. It has a large amount of $x = 2.81$ chemisorbed H_2O molecules in pores and high-energy molecular surfaces distributed through the pores. The pores support an activated molecular decomposition, $ZrO(OH)_2{\cdot}xH_2O \rightarrow ZrO_2 + (x+1)H_2O$, at low temperature ~85 °C, in a refined $ZrO_2{\cdot}\alpha H_2O$ amorphous structure (porous). A controlled reconstructive nucleation and growth by the amorphous state results in a new o-ZrO_2 metastable phase (an orthorhombic crystal structure) in near spherical shape of crystallites ($D = 15$ nm diameter) at 500 °C in 2 h. It converts to the usual m-ZrO_2, $D \geqslant 23$ nm, in baddeleyite ($P2_1/c$ monoclinic) crystal structure if raising the temperature to 800°C or above. A nonporous $ZrO(OH)_2{\cdot}xH_2O$ precursor, obtained by a similar process, involves the usual c-ZrO_2 (or t-ZrO_2) and m-ZrO_2 phase selection sequence on heating over these temperatures.

In comparison to the usual sol-gel process with hydrolysis by an alkoxide, this process is rather simple, economic, and easily controlled. This is processed in water. It represents a new so-gel process for fabricating refined metastable nanoceramics. Because of hydrolysis of metal cations (chlorides) dispersed in water and the reactivity of NH_4OH (a very cheap and easily available reagent), this process seems to be widely applicable to a variety of ceramics.

Acknowledgements

The authors gratefully acknowledge the financial support by a research grant from the Council of Scientific and Industrial Research (CSIR), Government of India.

References

[1] A. Feinberg, C.H. Perry, Structural disorder and phase transitions in ZrO_2–Y_2O_3 system, J. Phys. Chem. Solids 42 (1981) 513–518.
[2] M.I. Osendi, J.S. Moya, C.J. Serna, J. Soria, Metastable of tetragonal zirconia powders, J. Am. Ceram. Soc. 68 (1985) 145–149.
[3] T. Hirata, E. Asari, M. Kitajima, Infrared and Raman spectroscopic studies of ZrO_2 polymorphs doped with Y_2O_3 or CeO_2, J. Solid State Chem. 110 (1994) 201–207.
[4] T. Tsukada, S. Venigalla, A.A. Morrone, J.H. Adair, Low-temperature hydrothermal synthesis of yttrium-doped zirconia powders, J. Am. Ceram. Soc. 82 (1999) 1169–1174.
[5] A. Sturm, U. Betz, G. Scipione, H. Hahn, Grain growth and phase stability in a nanocrystalline ZrO_2–15 w.% Al_2O_3 ceramic, J. Nanostruct. Mater. 11 (1999) 651–661.
[6] L.M. Wang, S.X. Wang, R.C. Ewing, Amorphization of cubic zirconia by cesium-ion implantation, Philos. Mag. Lett. 80 (2000) 341–347.
[7] E. Djurado, P. Bouvier, G. Lucazeau, Crystallite size effect on the tetragonal–monoclinic transition of undoped nanocrystalline zirconia studied by XRD and Raman spectroscopy, J. Solid State Chem. 149 (2000) 399–407.
[8] R.H.J. Hannink, P.M. Kelly, B.C. Muddle, Transformation toughening in zirconia-containing ceramics, J. Am. Ceram. Soc. 83 (2000) 461–487.
[9] S. Ostanin, A.J. Craven, D.W. McComb, D. Vlachos, A. Alavi, M.W. Finnis, A.T. Paxton, Effect of relaxation on the oxygen K-edge electron energy-loss near-edge structure in yttria-stabilized zirconia, Phys. Rev. B 62 (2000) 14728–14735.
[10] S. Fabris, A.T. Paxton, M.W. Finnis, Relative energetics and structural properties of zirconia using a self-consistent tight-binding model, Phys. Rev. B 62 (2000) 6617–6630.
[11] S. Raghavan, H. Wang, W.D. Porter, R.B. Dinwiddie, M.J. Mayo, Thermal properties of zirconia co-doped with trivalent and pentavalent oxides, Acta Mater. 49 (2001) 169–179.
[12] D.D. Hass, A.J. Slifka, H.N.G. Wadley, Low thermal conductivity vapor deposited zirconia microstructures, Acta Mater. 49 (2001) 973–983.
[13] R.J. Moon, K.J. Bowman, K.P. Trumble, J. Rödel, Fracture resistance curve behavior of multilayered alumina–zirconia composites produced by centrifugation, Acta Mater. 49 (2001) 995–1003.
[14] D.M. Adams, S. Leonard, D.R. Russell, R.J. Cernik, X-ray diffraction of hafnia under high pressure using synchrotron radiation, J. Phys. Chem. Solids 52 (1991) 1181–1186.
[15] J.E. Lowther, Superhard materials, Phys. Stat. Sol. (b) 217 (2000) 533–543.
[16] J.E. Bailey, D. Lewis, Z.M. Libran, L.J. Porter, Phase transformations in milled zirconia, Trans. J. Br. Ceram. Soc. 71 (1972) 25–30.
[17] M. Qi, H.J. Fecht, Structural transition of zirconia during mechanical attrition, Mater. Sci. Forum 269-272 (1998) 187–192.
[18] I. Molodetsky, A. Navrotsky, M.J. Paskowitz, V.J. Leppert, S.H. Risbud, Energetics of X-ray-amorphous zirconia and the role of surface energy in its formation, J. Non-Cryst. Solids 262 (2000) 106–113.
[19] Y. Xie, Preparation of ultrafine zirconia particles, J. Am. Ceram. Soc. 82 (1999) 768–770.
[20] M.P. Klug, L.E. Alexander, X-ray Diffraction Procedure for Polycrystalline and Amorphous Materials, Wiley, New York, 1974.
[21] R.C. Mehrotra, Synthesis and reaction of metal alkoxides, J. Non-Cryst. Solids 100 (1988) 1–15.
[22] Y. Murase, E. Kato, Role of water vapor in crystallite growth and tetragonal–monoclinic phase transformation of ZrO_2, J. Am. Ceram. Soc. 66 (1983) 196–200.
[23] B. Xia, L. Duan, Y. Xie, ZrO_2 nanopowders prepared by low-temperature vapor-phase hydrolysis, J. Am. Ceram. Soc. 83 (2000) 1077–1080.
[24] S.M. Ho, On the structural chemistry of zirconium oxide, Mater. Sci. Eng. 54 (1982) 23–29.
[25] F.A. Cotton, G. Wilkinson, Advanced Inorganic Chemistry, Wiley-Interscience, 1962.
[26] M.J. Mayo, Processing of nanocrystalline ceramics from ultrafine particles, Int. Mater. Rev. 41 (1996) 85–115.
[27] S. Ram, G.P. Johari, Glass–liquid transition in hyperquenched metal alloys, Philos. Mag. B 61 (1990) 299–310.
[28] S. Ram, Calorimetric investigation of structural relaxation in supercooled $Ni_{75}Al_{22}Zr_2B$ amorphous alloy, Phys. Rev. B 42 (1990) 9582–9586.
[29] Powder Diffraction File JCPDS (Joint committee on powder diffraction standards), (International centre for diffraction data, Swarthmore, PA) 27-997 (c-ZrO_2), 24-1164 (t-ZrO_2) and 13-307 (m-ZrO_2).
[30] M.J. Buerger, X-ray Crystallography, John Wiley and Sons, 1990.
[31] H. Gleiter, Nanostructured materials: Basic concepts and microstructure, Acta Mater. 48 (2000) 1–29.